## AUTHOR QUERIES

AQ1 As per the TOC the chapter title is "Fluid-rock interactions in seals – impact on transport and mechanical properties". Please clarify which is the correct.

AQ2 As per project brief instruction, all the quoted emphasis has been changed to italics emphasis. Please check and confirm.

AQ3 Figure is blurred. Please supply better quality.

# 8

AQ1

# Fluid-Rock Interactions in Clay-Rich Seals: Impact on Transport and Mechanical Properties

**Elin Skurtveit[1,2], Rohaldin Miri[2], and Helge Hellevang[2,3]**


## ABSTRACT

Fluid-rock interaction in low-permeable clay-rich seal units is an important topic for the evaluation of the long-term seal integrity during geological storage of $CO_2$. In low-permeable sealing units, the diffusion of $CO_2$ into the matrix is a slow process, and studies of $CO_2$-initiated fluid-rock interaction in seals are challenging. In this paper, we present an overview of $CO_2$ transport mechanism and fluid-rock interaction processes that might alter mechanical and transport properties of seals. The review includes theoretical considerations and simulations, experimentally demonstrated processes, and field examples of flow and fluid-rock interaction in intact clay-rich seals as well as for fractures. For clay-rich seals dominated by minerals like quartz, illite, and smectite, the reactivity due to drop in pH is found to be low, and most reaction observed is found to involve calcite. Only minor porosity changes are observed, and implications for flow and $CO_2$ transport are uncertain due to limited data available. Swelling and shrinking property of smectites due to $CO_2$ sorption and $CO_2$ alterations within fractures in clay-rich seal is hardly addressed in the literature.


## 8.1. INTRODUCTION

AQ2 The interdependency between fluid-rock interactions, fluid flow, and mechanical properties of seals is an important aspect for understanding the long-term effects and risk of $CO_2$ sequestration. The requirement of a good seal is to keep $CO_2$ from migrating out of the reservoir, but unforeseen events of damage to the seal integrity, changing pressure conditions, or the need for remediation of damaged seals requires thorough understanding of fluid-rock processes within sealing units and their impact on fluid transport and mechanical properties. Clay-rich seals defined as shales and mudrock, characterized by their high content of clay minerals and small pore throats, provide good seals for $CO_2$ storage due to the high entry pressure and corresponding high capillary sealing. Typical properties of sealing units summarized by *Nordgård Bolås et al*. [2005] show pore throat diameter ranging from 9 to 1000 nm and corresponding permeabilities of $<10^{-6}$ and up to $10^{-3}$ mD ($10^{-21}$–$10^{-18}$ m$^2$). This covers the typical range of seal properties for existing $CO_2$ storage sites: for example, caprock permeability for the In Salah storage site is reported to be of the order of $10^{-22}$–$10^{-20}$ m$^2$ [*Armitage et al*., 2011]; at Sleipner, the pore throat radius is reported to be in the range of 14–40 nm and brine permeability in the range of $3–10 \times 10^{-19}$ m$^2$ [*Harrington et al*., 2009]; and caprock for the Snøhvit $CO_2$ storage site is reported to have an average permeability of 1–23 mD ($10^{-16}$ m$^2$) with many low-permeable shale layers [*Chiaramonte et al*., 2015].

$CO_2$ transport mechanisms and alteration processes discussed in this paper are summarized in Figure 8.1, showing increasing transport rates to the right. For an intact clay-rich sealing unit, the molecular-scale diffusion in pore water is typically a very slow process, whereas displacement-controlled volumetric Darcy flow in a connected pore


[1]*Norwegian Geotechnical Institute (NGI), Oslo, Norway*
[2]*Department of Geosciences, University of Oslo, Oslo, Norway*
[3]*The University Centre in Svalbard (UNIS), Longyearbyen, Norway*


*Geological Carbon Storage: Subsurface Seals and Caprock Integrity, Geophysical Monograph 238*, First Edition.
Edited by Stéphanie Vialle, Jonathan Ajo-Franklin, and J. William Carey.

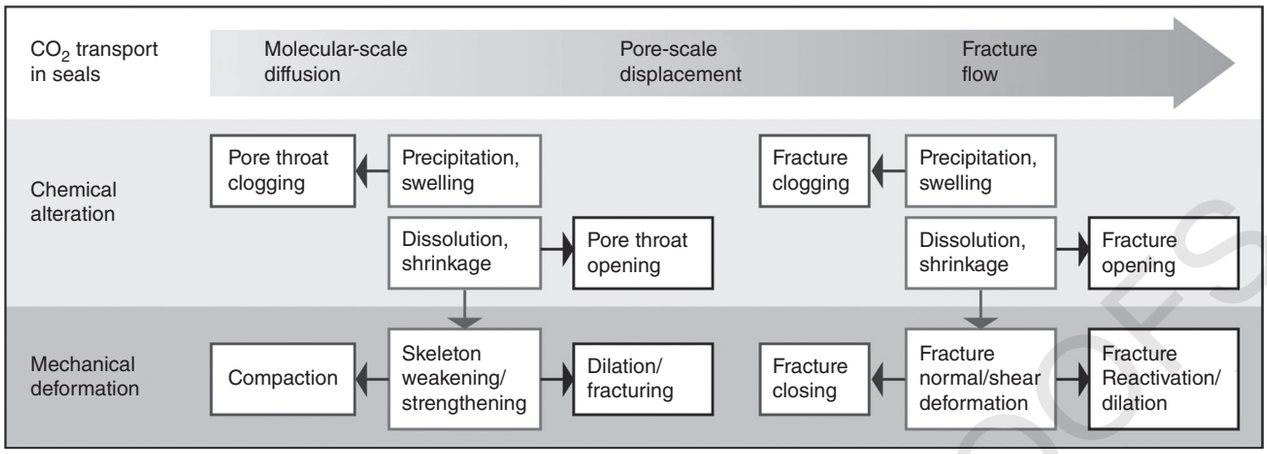


**Figure 8.1** $CO_2$ transport mechanisms with increasing transport rate to the right and schematic illustration of fluid-rock interaction mechanism and their implications for transport of $CO_2$ through low-permeable clay-rich units.

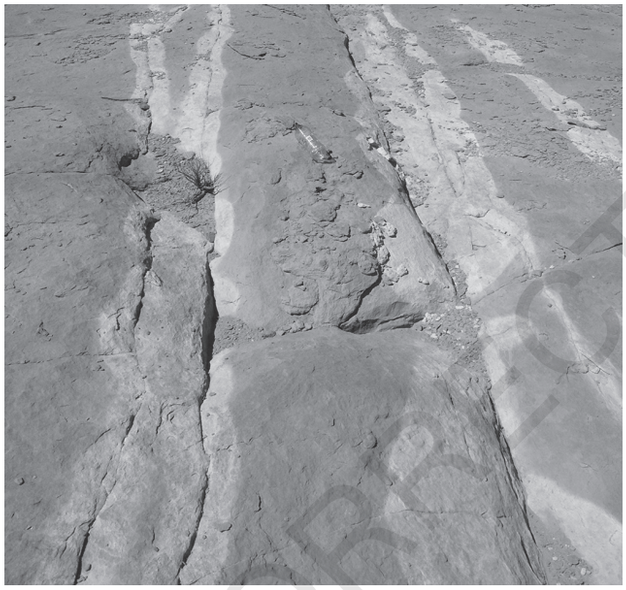

**Figure 8.2** Field example of fluid-rock interaction showing fracture parallel bleaching in permeable siltstone unit within the Entrada Formation, Utah. The bleached zone is found as a 1–10 cm thick zone along the fracture.

network is related to exceeding the capillary entry pressure [*Song and Zhang*, 2012] and may provide higher transport rates (Fig. 8.1). Further, outcrop-scale fractures are observed to provide conduits for migration of $CO_2$-saturated water (Fig. 8.2) in field outcrops like Green River, Utah, USA [e.g., *Kampman et al.*, 2012; *Shipton et al.*, 2004]. The role of microfractures in shales is less well understood [*Ougier-Simonin et al.*, 2016], providing a transition between pore-scale displacement and observed outcrop-scale fracture transport.

Fluid-rock interaction within a diffusive $CO_2$ front can be observed for $CO_2$ reservoir-seal boundaries [*Lu et al.*, 2009] and along faults and fractures within a leaking $CO_2$ system [e.g., *Shipton et al.*, 2004; *Ogata et al.*, 2014]. Dynamic interaction processes between fluid and rock involve processes of mineral dissolution, precipitation, and sorption. These processes may influence the transport properties for $CO_2$ in a sealing unit directly or cause alterations of the mechanical properties that induce deformation and changes in the transport properties (Fig. 8.1). In order to understand the complex interplay between flow, transport, chemical reactions, and mechanical changes, comparison of observations from various approaches is useful. Laboratory experiments give valuable input on the understanding of $CO_2$ transport mechanisms [e.g., *Wollenweber et al.*, 2010; *Skurtveit et al.*, 2012] and the fluid-rock reaction potential [e.g., *Alemu et al.*, 2011; *Liu et al.*, 2012; *Szabó et al.*, 2016] within laboratory limitations in time and conditions. Natural $CO_2$ field analogues can provide useful information about the long-term effects of materials being exposed to $CO_2$ or $CO_2$-enriched fluids and allow for back-calculation of reaction systems and rates [e.g., *Lu et al.*, 2009; *Kampman et al.*, 2014a, 2014b]. Geochemical kinetics of a $CO_2$-fluid-rock system can be simulated using reactive models [e.g., *Pham et al.*, 2011; *Hellevang and Aagaard*, 2013; *Hellevang et al.*, 2013; *Balashov et al.*, 2015; *Szabó et al.*, 2016] and provide information of long-term reaction potential in a system. Slow processes are challenging to quantify, and calibration of laboratory-determined transport and reaction rates with simulation and field observations is therefore critical to get a realistic model for the dynamic processes and implications for safe storage of $CO_2$ [*Kampman et al.*, 2014b]. Chemical interactions between injected $CO_2$, in

situ fluids, and the sealing unit might be positive for the seal integrity if they act to limit the fluid transport [e.g., *Balashov et al*., 2015] and reduce the potential for mechanical failure. On the other hand, fluid-rock interactions might also in some cases enhance the potential of fracturing of shales and increase the permeability [e.g., *Gherardi et al*., 2007; *Armitage et al*., 2013].

The occurrence of natural gas trapped under mudstone and shale structural or stratigraphic seals for millions of years is good evidence for the long-term integrity of this type of rock [*Van der Meer*, 2005]. Storage of $CO_2$ however differs from that of natural gas for a couple of reasons: First, natural gas is quite unreactive as a separate fluid phase or when dissolved in brines. $CO_2$, on the other hand, forms weak carbonic acid, lowering the pH typically to values between 3 and 5. The highest is observed when carbonate mineral dissolution buffers the pH change [*Pham et al*., 2011]. This pH drop leads to dissolution of silicate minerals present in the reservoir and the precipitation of secondary silicates (typically kaolinite and silica polymorphs) and secondary carbonates, mostly FeMgCa carbonates, and in some special cases, models predict dawsonite [*Pham et al*., 2011; *Hellevang and Aagaard*, 2013; *Hellevang et al*., 2013], although debated as it is rare in natural analogues. Second, the aqueous solubility of natural gas and $CO_2$ are different, and this affects their potential to diffuse into the seal. The solubility of natural gas components in brine, at the same temperature and pressure, is orders of magnitude lower than for $CO_2$ [*Miri et al*., 2014b]. In addition, gas solubility depends on the partial pressure rather than the total pressure, and because natural gas is generally a multicomponent mixture [*McCain*, 1990], their partial pressures may be quite low. $CO_2$, on the other hand, is injected as a nearly pure phase, and the partial pressure will be close to the total pressure. Third, $CO_2$ will typically be in a supercritical state, with high density and low viscosity.

The solubility of molecular $CO_2$ is controlled by the fluid pressure and temperature and the salinity of the aqueous solution and can be generally expressed as [*Hellevang*, 2006]

$$x_{CO_2} = \frac{P y_{CO_2} f_i}{K_H \gamma} \exp\left\{-\frac{v}{RT}\left(P - P_{sat}\right)\right\}, \qquad (8.1)$$

where $x$ and $y$ denote molar fractions of $CO_2$ in the aqueous and gas/supercritical phases, respectively; $P$ is the total pressure; $fi$ and $\gamma$ are the fugacity and activity coefficients for $CO_2$, respectively; $K_H$ is Henry's law constant; $v$ is the molar volume of $CO_2$; $R$ is the universal gas constant; $T$ is the absolute temperature; and subscript sat refers to the saturation pressure. It is not straightforward to see how the solubility is affected by temperature, pressure, and salinity, since both the fugacity and activity coefficients and Henry's law constant are temperature and pressure dependent. For typical $CO_2$ storage depths, the solubility increases with pressure and decreases with temperature, whereas the activity coefficient of $CO_2$ is unity for freshwater and increases with ionic strength, and dissolved salts therefore reduce the $CO_2$ solubility [e.g., *Spycher and Pruess*, 2005; *Miri et al*., 2014a]. Equation (8.1) and Henry's law only dictate the solubility of molecular $CO_2$ (hereafter referred to as $CO_{2,aq}$), whereas the total solubility (TIC) also depends on pH and the speciation of carbon into carbonate ($CO_3^{2-}$) and bicarbonate ($HCO_3^-$) ions. However, if speciation is ignored and pH is considered low (3–5), typical for normal $CO_2$ storage settings [*Pham et al*., 2011], the TIC can be well approximated by Eq. (8.1).

The $CO_2$ injected into a reservoir is expected to be supercritical $CO_2$ in the near vicinity of the injection well, surrounded by a mixing zone of supercritical $CO_2$ and formation water (brine) with a buffered pH. Further out from the injection, the $CO_2$ plume is expected to be fully saturated with water and acidified, whereas at the reservoir-caprock interface, the $CO_2$ plume is expected to be fully saturated with water or possible as a mixed zone. Dry supercritical $CO_2$ directly in contact with the caprock is considered unlikely, although possible if injection is close to the reservoir-caprock interface. As outlined above, the main mechanism for $CO_2$ transport into the caprock is expected to be molecular diffusion in the pore water from the zones where $CO_2$ is fully saturated with water or in a mixed phase, whereas advective flow in pore network or fractures will also be considered, although considered a less likely scenario for sites with proper pressure management.

The solubility of water in $CO_2$ is a function of temperature and pressure, and in the case of an upward migration through the seal, pressure and temperature conditions will change, and $CO_2$ will lose or take up water on the way [*Miri et al*., 2014a]. The solubility of water in $CO_2$ is shown for a range of temperatures (0–75°C) and pressures (1–300 bars) in Figure 8.3. Upward migration will lead to complex changes where the solubility will first decrease, before it will increase at the lower temperatures and pressures (Fig. 8.3). If $CO_2$ leakage rate is high, within fractures or fault zones, where the flow velocity might be high compared to $CO_2$ flow in porous media, adiabatic expansion of the gas leading to a further cooling compared to the shallower depth may also be expected [*Mao et al*., 2017]. However, this is not discussed in further detail in this paper.

Ensuring both short- and long-term integrity of seals is important for successful geological storage of $CO_2$. Key challenges related to the long-term integrity of clay-rich

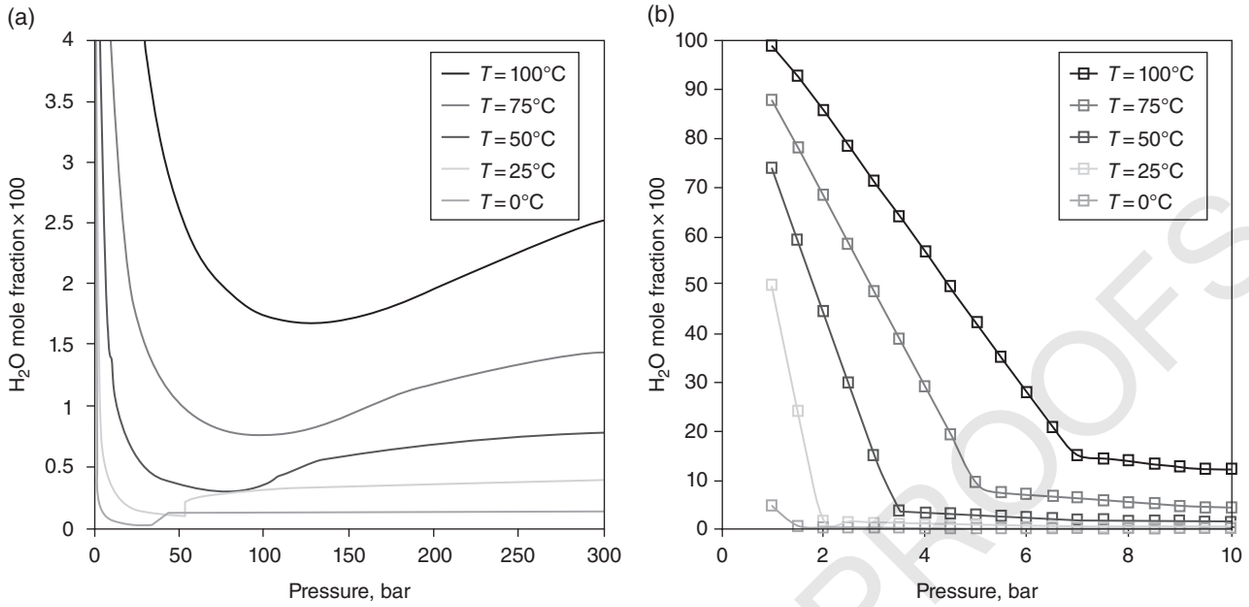


**Figure 8.3** Solubility of $H_2O$ in $CO_2$ as a function of temperature (0–100°C) and pressure. Reprinted with permission from *Miri et al*. [2014a]. Copyright (2014a) American Chemical Society. (a) Pressure range of 0–300 bar. (b) Details for pressure range of 0–10 bar, relevant during upward migration.

seals are to understand the mechanism for $CO_2$ transport into seals and the complex interplay between $CO_2$ fluid-rock interaction, alteration, and deformation that can alter the transport properties over time as outlined in Figure 8.1. Key challenges addressed in this paper include a review of theoretical models and laboratory experiments addressing interaction between $CO_2$ and clay-rich caprock material. Section 8.2 discusses $CO_2$ transport into clay-rich seals at the scale of molecular diffusion, pore-scale displacement, and fracture flow. Seal reaction such as precipitation, dissolution, and $CO_2$ adsorption will be reviewed with respect to $CO_2$ transport and deformation in Section 8.2.1, whereas Section 8.2.2 presents examples of fluid-rock interaction processes within selected sealing units of the North Sea. In the conclusion, the current knowledge and need for further research is summarized.

## 8.2. TRANSPORT OF $CO_2$ AND $CO_2$-SATURATED WATER

### 8.2.1. Diffusion-Dominated Matrix Transport

Dissolved $CO_2$ is transported into the seal by diffusion. The advancement rate of a diffusion front depends on the gradients of the dissolved inorganic carbon species and rock-specific factors such as the tortuosity and the potential of rock to consume $CO_2$ through chemical reactions such as $CO_2$ sorption and mineral dissolution and growth. The effect of the tortuosity and reactions on the diffusion rates of the carbon species can be seen in the reaction-diffusion equation:

$$\frac{\partial C_i}{\partial t} = D_{e,i}\nabla^2 C_i - R_c, \tag{8.2}$$

where $C_i$ is the concentration of dissolved carbon species i, $t$ is time, $D_{e,i} = \phi D_i^0 / \tau$ is the effective diffusion coefficient, $D^0$ is the bulk water diffusion coefficient, $R_c$ is a reaction term, with positive values indicating uptake into the solid framework, $\phi$ is porosity, and $\tau$ is tortuosity. A more tortuous path offers more contact time between $CO_2$ and resident brine, resulting in better mixing and enhanced solubility in the system [*Rathnaweera et al*., 2016]. Similarly, reactions reduce the mass of the free-phase $CO_2$, further retarding the rate of plume migration [*Xu et al*., 2003, 2005].

The diffusion coefficient for $CO_2$ in a brine-saturated caprock sample may be measured experimentally. Experimental investigation of $CO_2$ diffusion in the Muderong Shale, Australia, provided effective diffusion coefficients of $3.08–4.81 \times 10^{-11}$ m²/s at reservoir conditions ($T = 45–50$°C and $P < 20$ MPa) [*Busch et al*., 2008]. Repetitive $CO_2$ diffusion experiments on clay-rich marlstone from the Upper Cretaceous caprock sequence of the Münsterland Basin show an increase in the effective diffusion coefficient from $7.8 \times 10^{-11}$ to $1.2 \times 10^{-10}$ m², indicating a change in transport properties during the experiment [*Wollenweber et al*., 2010]. Diffusion into intact mudstones/shales is a very slow process, and

uncertainties are related to the upscaling of experimental data. Diffusion rates may also be estimated from studying natural analogues. One such analogue is $CO_2$ diffusion from the North Sea Brae Formation into the Kimmeridge Clay [*Lu et al.*, 2009]. Here carbon isotopes indicate that dissolved $CO_2$ has reached approximately 12 m into the caprock matrix over 70–80 million years. Assuming $CO_2$ a conservative tracer, this suggests an effective diffusion coefficient of $10^{-14}$ m²/s (Fig. 8.4). Such a low effective diffusion coefficient indicates either very low values of the tortuosity or that the mudstones acted as a sink for the $CO_2$ species, thereby slowing down the transport. The Kimmeridge Clay is rich in organic matter [*Tribovillard et al.*, 1994], and $CO_2$ interaction with the mudstone is therefore one likely reason for the slow transport. The lower diffusion rate of the field analogue (Kimmeridge Clay) compared to the laboratory rates might be material dependent but could also be an indication that the diffusion under in situ condition and for long term is restricted by some factors that are less active in the laboratory experiments. Possible sample damage due to dehydration or unloading of laboratory samples might also contribute to the higher diffusivity observed at laboratory scale.

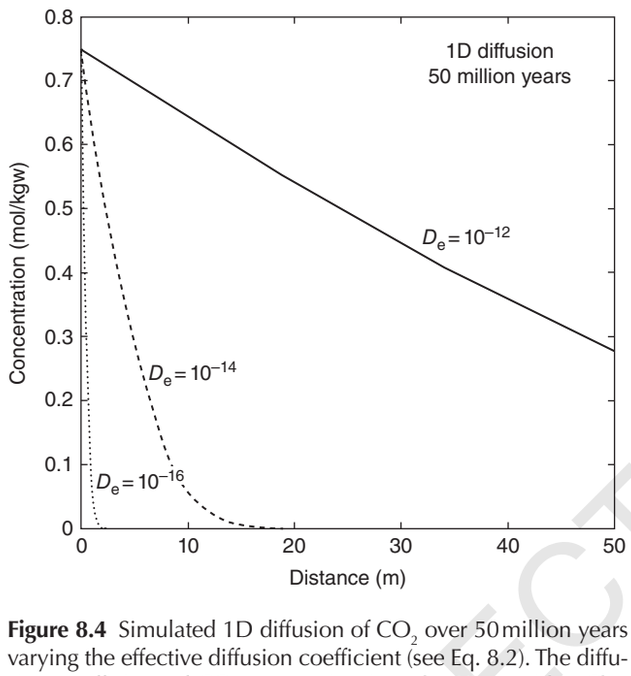


**Figure 8.4** Simulated 1D diffusion of $CO_2$ over 50 million years varying the effective diffusion coefficient (see Eq. 8.2). The diffusion coefficient of $CO_2$ penetrating into the Kimmeridge Clay (12 m over 70–80 million years) can be approximated to be $10^{-14}$ m²/s based on this model.

Diffusion fronts are sometimes observed to be sharp and sometimes diffuse, which provide valuable insights regarding timescale and length scale of the underlying mechanisms of $CO_2$ transport and the nature of the $CO_2$-brine-rock reactions. The type of diffusion front can be explained by the relative rates of diffusion and reactions (Eq. 8.2). If reactions are very fast compared to diffusion ($R >> D_{e,i}\nabla^2 C_i$), a sharp front will develop, whereas diffuse fronts develop when reactions are very slow compared to diffusion ($R << D_{e,i}\nabla^2 C_i$). Both diffuse and sharp diffusion fronts are easily observed in bleached siltstone in Utah [*Busch et al.*, 2014] (Fig. 8.5). Diffusion in mudstones is commonly very slow, and reactions can be fast compared to the diffusion, so sharp fronts are expected in shales and mudstones.

### 8.2.2. Capillary Entry Pressure and Displacement Flow

Gaseous or supercritical $CO_2$ is prevented from entering intact (non-fractured) mudstones or shales due to high capillary entry pressures. The capillary entry

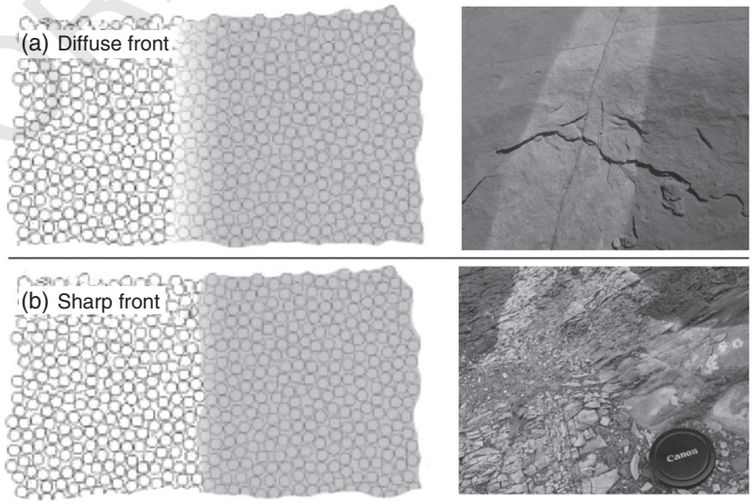


**Figure 8.5** Difference between diffuse (a) and sharp (b) reaction fronts.

pressure, $P_c$, can be obtained from the Young-Laplace equation [*Washburn*, 1921]:

$$P_c = P_{CO_2} - P_w = \frac{2\gamma \cos\theta}{r}, \tag{8.3}$$

where $r$ is the median pore throat radius, $\gamma$ is the interfacial tension between the wetting and non-wetting fluids, and $\theta$ is the wettability angle between the wetting and non-wetting fluid and the host rock. In general, clay-rich seals with lower permeability (i.e., smaller median pore throat sizes) have higher capillary entry pressures, and therefore, they pose higher resistance against $CO_2$ invasion. The $CO_2$-water interfacial tension has been measured for relevant $CO_2$ storage conditions by *Chiquet et al*. [2007].

Capillary entry pressure for $CO_2$ can also be measured directly in the laboratory. Comparison of methods for determining capillary entry pressure is discussed by *Boulin et al*. [2013], showing differences in time and accuracy. For $CO_2$, experimentally measured capillary entry pressure (or displacement pressure) is in the range of 0.1–5 MPa for a selection of intact mudrock samples [*Hildenbrand et al*., 2004] and 3.5–4.3 MPa for shale from the Draupne Formation in the Troll East area [*Skurtveit et al*., 2012]. The measured $CO_2$ displacement pressure is found to be lower than for natural gas ($CH_4$) and nitrogen ($N_2$) [*Hildenbrand et al*., 2004]. Effective Darcy permeability for $CO_2$ has been studied in the same experiments as for $CO_2$ entry pressure. High confining pressure was applied in order to avoid hydro-fracturing of the sample, and Darcy flow was imposed upon shale samples in the experiments by *Hildenbrand et al*. [2004], where a slight decrease in effective $CO_2$ permeability (range of $10^{-18}$–$10^{-24}$ m$^2$) was measured compared to the water permeability (range of $10^{-19}$–$10^{-21}$ m$^2$). In these experiments, a high pressure gradient (exceeding the expected breakthrough pressure) was imposed across the sample, and the resulting gas flux was monitored by means of pressure change. No mechanical changes (i.e., fracturing) were reported. *Skurtveit et al*. [2012] measured effective $CO_2$ permeability of the order of $10^{-21}$ m$^2$, within the same order of magnitude as for brine permeability; however, the effective $CO_2$ permeability was found to be dependent on volumetric dilation in the sample, and a microfracture-dominated flow was interpreted.

### 8.2.3. Fracture Transport

The $CO_2$ entry pressure for fractures can also be provided by Eq. (8.3), but with the pore throat radius replaced by $b$, the initial fracture aperture [*Wang and Peng*, 2014]. The most common model to describe single-phase flow through microfractures is given by the Navier-Stokes equations which express conservation of momentum and mass over the fracture with impermeable walls. The laminar flow of an incompressible Newtonian fluid with constant viscosity may be written as [*Bird*, 2002]

$$\rho\left(u.\nabla\right)u = \mu\nabla^2 u - \nabla e,\ \nabla.u = 0, \tag{8.4}$$

where $\rho$ is the fluid density, $\mu$ is the fluid viscosity, u is the velocity vector, and $e(x,y,z)$ is the fluid potential (i.e., the mechanical energy per unit mass). Assuming that (i) the fracture is composed of two parallel plates separated by a small aperture, (ii) the variability in fracture aperture is minimal, and (iii) the inertial forces are much smaller compared with the viscous and pressure forces, Eq. (8.3) reduces to the so-called local cubic law (LCL) [*Zimmerman and Bodvarsson*, 1996; *Oron and Berkowitz*, 1998]:

$$\nabla.\left(\frac{b^3}{12\mu f}\nabla e\right) = \nabla.\left(T_f \nabla e\right) = 0, \tag{8.5}$$

where *Tf* is the transmissivity of fracture and $f$ is the correction accounted for fracture roughness. Several studies have considered the validity of the LCL, and it has been shown that for the Darcian flow (Reynolds << 1), inertial term can be safely ignored [*Walsh*, 1981; *Renshaw*, 1995; *Zimmerman and Bodvarsson*, 1996; *Brush and Thomson*, 2003]. Furthermore, it has been shown that the assumption (ii) can be relaxed if aperture are measured as an average over a certain length. Equation (8.5) shows that fracture conductivity is proportional to the cube of mean aperture and that flow rate ($Q$) is directly proportional to the fluid potential and can be written as

$$Q = -\frac{b^3}{12\mu f}\nabla e, \tag{8.6}$$

As Eq. (8.6) shows, the fracture transmissivity decreases as the aperture size reduces, indicating that fracture flow of $CO_2$ is mainly controlled by the aperture size. The ability for a fracture to deform and change its aperture is given by the normal stiffness $K_n$ given as

$$K_n = \frac{d\sigma}{d\delta} \tag{8.7}$$

where $d\sigma$ is the change in stress and $d\delta$ is the corresponding fracture deformation [*Jaeger et al*., 2009]. Characteristic nonlinear behavior for fracture stiffness is demonstrated experimentally as well as in conceptual models [e.g., *Bandis et al*., 1983; *Myer*, 2000; *Pyrak-Nolte and Morris*, 2000] and explained by the increasing contact area in the fracture as the normal load increases. There is a large amount of work dealing with the correlation between

applied stress conditions, fracture aperture, porosity, and the corresponding fracture permeability [e.g., *Barton et al*., 1985; *Cho et al*., 2013] as well as for permeability in fault zones [e.g., *Faulkner et al*., 2010] that will not be further discussed in this review.

A complex interplay of chemical and mechanical factors controls the fracture aperture. Experimental evidence supports the movement of $CO_2$ in low-permeability shale matrices via fractures created from excess gas pressure. Direct laboratory measurements of $CO_2$ entry, breakthrough, and flow in an initially brine-saturated shale caprock have been described in *Angeli et al*. [2009] and *Skurtveit et al*. [2012], where the $CO_2$ breakthrough was recognized by a marked dilation of the test sample. Effective $CO_2$ permeability as a function of strain could be fitted to a model where the measured dilation (strain) represents a change in fracture aperture [*Olivella and Alonso*, 2008]. The effective $CO_2$ permeability observed after the $CO_2$ breakthrough was found to be more sensitive to changes in volumetric deformation than the absolute brine permeability, and it could be fitted to a power law dependency [*Skurtveit et al*., 2012]. This supports experimental work by *Harrington and Horseman* [1999], suggesting that microfractures link up to form a distinct pathway through the low-permeable seal units in their gas breakthrough experiments on Boom clay and bentonite. *Edlmann et al*. [2013] suggested a critical fracture aperture: below this critical fracture aperture, there is little or no $CO_2$ flow along the fracture, nor in gaseous or supercritical state, close to or at the critical aperture, only gaseous $CO_2$ will flow, whereas above the critical fracture aperture, both $scCO_2$ and gaseous $CO_2$ will potentially flow. Yet quantitative description of the threshold aperture size is not provided. The variation of the fracture aperture size induced by chemical interaction between $CO_2$ and the host rock (e.g., mineralization, dissolution, desiccation, swelling, etc.) may enhance/decrease the sealing capacity. The advection of $CO_2$ after breakthrough supports water evaporation into $scCO_2$, increasing capillary suction, leading to additional sediment contraction and consequently formation of capillary-driven fractures [*Espinoza and Santamarina*, 2012; *Schaef et al*., 2012]. In addition, the two-phase flow of $CO_2$ and brine in the fracture network modifies the capillary entry pressure of the fracture network and the sorptive chemistry within the shale matrix. In order to describe the two-phase flow of $CO_2$ and brine in the fracture network, it is needed to take into account the characteristics of multiphase flow such as relative permeabilities and capillary pressure between water and $CO_2$ that may affect the local deformation of the shale caprocks [*Gherardi et al*., 2007; *Wang and Peng*, 2014]. This can be solved using a dual-porosity model in which the discontinuous nature of porosity and permeability is avoided by replacing them locally by their average values. Moreover, it may be assumed that there is only viscous flow in the fracture network (sink) and the matrix will act as a source term in the fracture flow equation [*Warren and Root*, 1963]:

$$\varnothing_{\mathrm{f}} \frac{\partial S_{\alpha \mathrm{f}}}{\partial t} + T_{\mathrm{mf}_\alpha} = -\nabla . u + R_\alpha , \tag{8.8}$$

where $S$ is phase saturation, $t$ is time, $\varnothing$is the fracture porosity, $u$ is phase fluid Darcy velocity, $R$ is fluid source/sink term, and $T$ is the transfer function defining the interaction between matrix and fracture (see next section). The subscript $\alpha$ refers to either the wetting (water) phase or the non-wetting ($CO_2$) phase. The subscripts m and f represent the matrix and the fracture, respectively. Darcy's velocity of phase $\alpha$ is given by

$$u_\alpha = -\lambda_\alpha k_{\mathrm{f}} \nabla e_\alpha , \tag{8.9}$$

where $k_{\mathrm{f}}$ is the fracture absolute permeability given by the cubic law and $\lambda\alpha$ is the fluid mobility and is equal to the ratio of the relative permeability $k_{\mathrm{r}}\alpha$ and the dynamic viscosity.

Only limited experimental data are available on permeability of fractured shale and even less on permeability of $CO_2$ in fractures. *Carey et al*. [2015] measured the peak permeability of 900 mD for well-defined bedding parallel fractures, compared to 30 mD for the more complex fracture patterns formed across the bedding in a triaxial and direct shear device for the calcite-rich Utica shale core from Ohio and Pennsylvania. A naturally fractured and carbonate-cemented fracture from Kimmeridge shale, UK, was tested for flow properties in a direct shear device after artificially separated and demineralized (carbonate mineralization removed by acid) [*Gutierrez et al*., 2000]. The test showed that increasing normal contact stress across the fracture lowered the water permeability in an exponential way. However, the fractures were not entirely healed, and permeability remained higher than the matrix permeability for the test period of hours. In general, fracture transmissibility is strongly controlled by the ductility index, defined as the effective mean stress normalized to the tensile strength of the intact rock [*Ishii*, 2015]. This means that the experimentally measured fracture permeability is highly dependent on the effective stress condition used in addition to the shale properties. For ductile shales and clays, the consolidation, creep, and swelling may close fractures during an experiment [*Zhang*, 2011] and the capillary entry pressure for fractures to be close to that of the matrix. This highlights the need for use of relevant pressure condition when considering $CO_2$ transport properties for fractures.

### 8.2.4. Fracture-Matrix Interactions

In the case of a two-phase displacement flow in a fracture network, fracture-matrix interactions may alter the dynamic of the flow process and even immobilize $CO_2$ that has migrated into the caprock along the fractures. Due to high fracture permeability, the fluids in the interconnected fracture network will quickly be displaced by $CO_2$, while the shale matrix remains water saturated [*Saidi*, 1983; *Wang and Peng*, 2014]. The fracture-matrix flow term, *Tmf* in Eq. (8.8), represents the volumetric flux of the fluid from the matrix blocks into the fractures (per unit time and per unit volume of the reservoir), and it is given as [*Barenblatt et al*., 1960]

$$-T_{\mathrm{mf}_\alpha} = \phi_{\mathrm{m}} \frac{\partial S_{\alpha \mathrm{m}}}{\partial t} \tag{8.10}$$

During a $CO_2$ invasion into the fracture network, different mechanisms may come into play, such as clay swelling, gravity drainage, $CO_2$ diffusion and sorption, and matrix drying [*Busch et al*., 2010]. Generally, the pressure in the matrix, $P_{\mathrm{m}}$, follows the overburden gradient, while the pressure in the fracture network, $P_{\mathrm{f}}$, is controlled by the height of $CO_2$ column in contact with caprock. Considering the high compressibility of $CO_2$ in either gaseous or a supercritical state, the pressure differential between the fractures and the matrix creates a driving force leading to matrix depletion [*Saidi*, 1983; *Lim and Aziz*, 1995], given as

$$T_{\mathrm{mf}_\alpha}^{\mathrm{expansion}} = \sigma \lambda_\alpha \left[ P_{\mathrm{f}} - P_{\mathrm{m}} \right] \tag{8.11}$$

where $\sigma$ is the shape factor which represents the mean flow path between the matrix and its corresponding fracture [*Warren and Root*, 1963]. When $CO_2$ invades the fractures surrounding the water-saturated matrix, water may drain downward due to the density difference between $CO_2$ and water. This mechanism is referred to as gravity drainage. However, the capillarity (matrix) will act against this mechanism and retain water in the matrix. Since the shale matrix usually has high capillary threshold, it is very unlikely that $CO_2$-water gravity drainage occurs during $CO_2$ invasion into the caprock [*Festoy and Golf-Racht*, 1989; *Rossen and Shen*, 1989]. In addition to the gravity drainage flow, the pressure-driven flow (Eq. 8.11) will occur only when the $CO_2$ pressure exceeds the summation of reservoir pressure and capillary entry pressure. Nevertheless, in a capillary sealing case, other mechanisms will come into play, transferring $CO_2$ into the fracture-matrix system.

$CO_2$ may exist in several forms in the caprock: (i) as a free phase displacing water in the fracture network, (ii) as an absorbed/adsorbed phase onto the matrix, and (iii) dissolved in brine diffusing into the shale matrix. The role of free-phase $CO_2$ is already included in Eq. (8.8). The mass of $CO_2$ adsorbed in the fracture network can be calculated based on the Langmuir isotherm [*Wang and Peng*, 2014]. However, it may be reduced if the invaded $CO_2$ is sufficiently dry to partly evaporate the adsorbed water films. Nevertheless, the extent of dehydration will depend on the water content of the $CO_2$, and complete evaporation of adsorbed water films on the fracture surface is not very likely to occur in a $CO_2$ storage scenario due to strong adhesive solid–liquid interactions [*Espinoza and Santamarina*, 2012; *Giesting et al*., 2012; *Schaef et al*., 2012]. $CO_2$ diffusion and sorption into the matrix is an important mechanism which may reduce the risk of leakage given the high adsorption capacity of clay minerals [*Busch et al*., 2008]. *De Jong et al*. [2014] have performed several unconfined volumetric strain measurements in smectite-bearing fault material and found that $CO_2$ penetrating into fracture/joint walls can be expected to cause swelling of a few percent (≈3%), reducing fracture apertures and thus reducing bulk permeability (≈11% calculated using Eq. (8.6)), thereby improving seal integrity. The mass exchange rate of gas sorption from the shale matrix to the fracture network depends on the difference between the matrix gas content and the equilibrium gas, and it is expressed by *Wang and Peng* [2014] as

$$T_{\mathrm{mf}_\alpha}^{\mathrm{diffusion}} = \frac{-\rho_{\mathrm{ga}} \rho_{\mathrm{c}}}{\sigma D} \left[ m_{\mathrm{b}} - m_{\mathrm{e}} \left( P_{\mathrm{f}} \right) \right] \tag{8.12}$$

where $\rho_{\mathrm{ga}}$ is the gas density under the standard conditions and $\rho_{\mathrm{c}}$ is the bulk density of the shale; $m_{\mathrm{b}}$ and $m_{\mathrm{e}}$ are the current and equilibrium gas content at fracture pressure, $P_{\mathrm{f}}$, respectively; and $D$ is the effective diffusion coefficient of gas. *Busch et al*. [2008] have reported the sorption capacity of the Muderong shale and various clay minerals (kaolinite, illite, smectite) from Western Australia to about 1.0 mmol/g. *Wollenweber et al*. [2010] have performed similar sorption experiments on marlstone and reported sorption capacities of 0.27 mmol/g, which is slightly lower than the sorption capacity reported by *Busch et al*. [2008] and assigned to the higher organic content of the samples investigated by *Busch et al*. [2008]. Likewise, significantly higher sorptive uptake is reported for coals owing to high organic matter content [e.g., *Weniger et al*., 2010; *Chareonsuppanimit et al*., 2012]. In addition, the sorption capacity is a function of specific surface area (see Eq. 8.12) accessible for $CO_2$ to be in contact with matrix blocks. Smaller fracture spacing in shale implies smaller matrix block sizes and higher specific surface areas, hence intensified exchange rates for the sorbed gas.

## 8.3. SEAL REACTIONS AND IMPLICATIONS FOR FLOW AND DEFORMATION

### 8.3.1. $CO_2$-Shale Reactivity

As $CO_2$ diffuses into the rock matrix from the base of the seal or along a non-sealing fracture or heterogeneity, minerals will react and secondary phases may form [e.g., *Gaus et al*., 2005]. The rate of the reactions will be controlled by both the diffusivity and the sink/source reactions as outlined in Eq. (8.2) (Section 8.2). In order to define the reaction, major minerals that will affect $CO_2$ diffusion over long timescales need to be defined, and the mineral kinetic parameters (kinetic constants, reactive surface areas) must be known for all mineral phases taking part in the reactions. There has been progress in understanding the parameterization and uncertainty of kinetic simulations [*Hellevang and Aagaard*, 2013; *Hellevang et al*., 2013], but especially reactive surface areas are still very difficult to estimate.

Compared to kinetic modeling studies for reservoirs, only a limited number of kinetic models are addressing seals with a clay-dominated composition (see Table 8.1 for an overview). Reactive diffusive transport modeling calculations for clay-dominated seals predict a decrease in porosity due to kaolinite precipitation [*Gaus et al*., 2005] and chlorite-to-ankerite transformation [*Balashov et al*., 2015], whereas the reactivity of quartz and clay minerals (illite and smectite) is low. However, modeling by *Tambach et al*. [2015] predicts porosity increase at the reservoir contact mainly due to siderite dissolution. Simulations by *Gherardi et al*. [2007] on carbonate-rich shales suggest that during fully liquid-saturated conditions in a diffusion-controlled regime, pH will be buffered and calcite precipitation occurs, whereas calcite dissolution can occur in the caprock if a free, water-rich $CO_2$-dominated phase migrates into the caprock through discontinuities. Although differences in alteration are observed for a diffusion-dominated caprock matrix system and a fractured caprock with flow and possibly free $CO_2$ phase, the reactions observed are mainly calcite dominated and might not be of high relevance for the clay-rich seals.

The geochemical reactions to be expected from mineral reactions due to the reduced pH during dissolution of $CO_2$ into the pore fluid may be addressed in experimental work. Reaction experiments on shale and mudstone as summarized in Table 8.2 show only limited reactions in the shale, mainly nucleation and growth of carbonate and smectite [*Kaszuba et al*., 2005; *Carroll et al*., 2011], whereas observed illite-smectite transformation into illite might be due to heating [*de Lima et al*., 2011]. In general, carbonate-rich shale is more reactive than clay-rich shale [*Alemu et al*., 2011], showing dissolution of plagioclase and clay minerals (illite and chlorite) and precipitation of smectite.

Variations in matrix porosity can also be observed within geochemical alteration experiments on cuttings [*Mouzakis et al*., 2016] and diffusion experiments [*Busch et al*., 2008; *Wollenweber et al*., 2010]. Experimental work on low-permeable caprock is time consuming and challenging due to the slow transport properties. Detection of chemical alteration and porosity changes with following changes in transport properties over time is not straightforward, and there is some spread in the reported experimental results (Table 8.2). Diffusion and sorption experiments by *Busch et al*. [2008] show dissolution of silicates and precipitation of carbonates to have measurable effects on the porosity, permeability, and diffusion properties of the Muderong Shale (Australia), with a tendency to enhance the transport properties. However, the effect of porosity increase on transport properties might also be related to the preferential dissolution of pores or pore throats. Caprock samples from the In Salah injection site show dissolution of siderite and chlorite from both pores and pore throats, and the increase in pore throat radii is used to explain the factor 8 permeability increase observed after the flooding with $CO_2$-saturated water [*Armitage et al*., 2013].

Matrix properties, such as mechanical strength and stiffness, control matrix deformation response to stress. Conventional triaxial tests [e.g., *Berre*, 2011] are the most common method to address the mechanical strength of intact rock samples. There are a limited number of tests that have addressed potential modifications to the mechanical properties of rock samples due to $CO_2$ interaction by comparing the deformation moduli and mechanical strength of altered and unaltered samples, but most experimental work is on reservoir sandstone [e.g., *Le Guen et al*., 2007; *Hangx et al*., 2013] and is summarized in *Rohmer et al*. [2016]. The design of experimental programs capturing alteration-induced geomechanical changes is even more challenging for caprocks due to the low permeability and slow transport of $CO_2$ solutions into the rock. The long-term fate of $CO_2$ alteration of sealing units has been addressed using the Green River natural analogue in Utah [*Kampman et al*., 2013; *Busch et al*., 2014]. The study, comparing mechanical strength of unreacted and reacted (bleached) samples, concluded that the variation in depositional environment and porosity imposed a strong control on rock strength, whereas mechanical changes related to the observed bleaching cannot be documented [*Busch et al*., 2014]. However, mechanical degradation related to long-term $CO_2$ exposure has been documented using indentation and scratch testing of the Entrada Sandstone and Summerville Siltstone, Utah [*Sun et al*., 2016]. This micro-mechanical test method provides an evaluation of

**Table 8.1** Overview of Simulations Addressing Reaction in Clay-Rich Caprocks and Effects on Porosity and Transport.

| Formation/field | Method | Caprock minerals | Observed reactions | Effects on porosity and transport | Reference |
|---|---|---|---|---|---|
| Nordland Shale Sleipner, North Sea | Kinetic batch modeling PHREEQC and reactive transport modeling Conditions: 37°C and $101.3 \times 10^5$ Pa | Mass %: illite (24.7), kaolinite (18), quartz (21.5) plagioclase (12.4), smectite (8.8), calcite (1), chlorite (4.1), K-feldspar (2.1), pyrite (2.8), siderite (1.6), mixed layer clay (1.4) | Dissolution of calcite, feldspar alteration; apart from kaolinite precipitation, the reactivity of the clays (illite, smectite, etc.) is low | A decrease in porosity is <3% in 15 000 years, and improved sealing is modeled, whereas in some scenarios carbonate dissolution might induce a slight porosity increase at the bottom of the caprock, but without ability to migrate into the caprock | *Gaus et al.* [2005] |
| Chlorite- and illite-containing seal, close to the Marcellus Formation (USA) in composition | Reactive diffusion model MK76. Conditions 348.15 K and 30 MPa | Vol.%: quartz (38.41), illite (33.13) chlorite (13.76), calcite (4.93), microcline and pyrite | Transformation of chlorite to ankerite is the dominant reaction occluding the shale porosity. Quartz is almost inert. Reactions of feldspars and clays depend strongly on their reaction rate constants | A decrease in porosity is modeled from the initial 5% to 0% in 6–14,000 years | *Balashov et al.* [2015] |
| Shale from depleted gas reservoir offshore the Netherlands | 1D kinetic diffusion modeling with PHREEQC for caprock | Vol.%: quartz (63.1), illite (10.1), dolomite (11.4), anhydrite (6.5), albite (2.9), K-feldspar (3.9), pyrite (0.3), siderite (1.7) | pH is partially buffered by dissolution of siderite, albite, and microcline, which are transformed into Fe-illite and quartz | Porosity increases from 5.0 to 5.7% at the reservoir contact during 10.000 years, and the $CO_2$ diffusion is 6.4–12.9 m into the caprock for the same time | *Tambach et al.* [2015] |
| Carbonate-rich shales from onshore gas reservoir in the north of Italy | Diffusion in the aqueous phase and gas and/or liquid advection. Batch simulations using TOUGHREACT / TOUGH2 | Calcite (0.3), dolomite (0.03), quartz (0.2), muscovite (0.19), smectite (0.15) | Dissolution and precipitation reactions involving calcite dominates. Clay dissolution of illite, chlorite, and muscovite and precipitation reactions (Na-smectite) less significant | For a free $CO_2$-dominated phase in fractures, significant calcite dissolution and porosity enhancement are predicted. For diffusion, some calcite precipitation is predicted which leads to further sealing of the storage reservoir | *Gherardi et al.* [2007] |

**Table 8.2** Overview of Experimental Work Addressing Reaction in Clay-Rich Caprocks and Effects on Porosity and Transport.

| Formation/field | Method | Caprock minerals | Observed reactions | Effects on porosity and transport | Reference |
|---|---|---|---|---|---|
| **Geochemical batch reaction work** | | | | | |
| Silurian Maplewood Shale, an argillaceous shale from Monroe County, New York, USA | Experimental work in reaction cell | Vol.%: clay minerals like phyllosilicates illite, mica (65), quartz (27), feldspar (5), chlorite (2), pyrite | Nucleation and growth of siderite on shale suggests the aquitard is a reactive component in the system | Not discussed | *Kaszuba et al.* [2005] |
| Shale caprock, Krechba Field, In Salah, Algeria | Cement-rock-brine-$CO_2$ experiments | Wt.%: illite (44), chlorite (30), quartz (20), albite, dolomite, kaolinite, siderite | Little indication of alteration of the shale by $CO_2$-rich brines; only small precipitates on the shale surface.<br>Added cement gives more extensive clay dissolution and precipitation of smectite and calcium carbonate | Not discussed | *Carroll et al.* [2011] |
| Palermo shale caprock, Paraná Basin, Southern Brazil | Experimental work, pressurized cells, reservoir conditions | — | Transformation from illite-smectite to illite | Not discussed | *de Lima et al.* [2011] |
| Carbonate-rich shale, De Geerdalen Fm, and clay-rich shale, De Geerdalen Fm, Svalbard | Batch reaction experiments | Carbonate-rich shale Wt.%: quartz (13), calcite (29), illite (22), chlorite (38), ankerite (7), plagioclase/albite (6)<br>Clay-rich shale Wt.%: quartz (26), illite (26), chlorite (19), plagioclase/albite (8), siderite (5), pyrite | Carbonate-rich shale: dissolution and re-precipitation of carbonates; dissolution of plagioclase, illite, and chlorite; and the formation of smectite<br>Clay-rich shale: no significant mineralogical alterations except for dissolution of silicate minerals | Not discussed | *Alemu et al.* [2011] |
| Marine Tuscaloosa Shale, Mississippi | Fixed volume reactors | Quartz (60%), feldspar (14%), chlorite (9%), kaolinite (5%), illite (5%), calcite (5%) | Mineral dissolution under $CO_2$ sequestration conditions | Total porosity increased slightly but connected porosity decreased | *Mouzakis et al.* [2016] |
| **Combined transport and geochemical work on intact samples** | | | | | |
| Muderong Shale, Australia | Experimental work on diffusive transport and gas sorption | Illite-smectite (27%), smectite in I-S (20%), mica/illite (8%), kaolinite (26%), quartz (27%), chlorite (5%), siderite (2%), orthoclase (3%), pyrite (2%) | Dissolution of silicates and precipitation of carbonates | Tendency to enhance the transport properties | *Busch et al.* [2008] |
| **Combined transport and geochemical work on fractured samples** | | | | | |
| Fractured claystone, Upper Toarcian Formation, Tournemire, France | 25°C in flow-through reactor with confinement of 0.12 MPa | Vol.%: calcite (25), siderite (2), quartz (25), clay minerals (45), and pyrite (3)<br>Clay fraction: kaolinite (24), micas (muscovite) (10), interstratified illite-smectite (10), and chlorite (1) | Calcite and some quartz grain dissolution, altering of fracture surface | Sole seepage of $CO_2$-brine through a fracture does not alter permeability, while cycling flow of $CO_2$-gas and $CO_2$-brine increases fracture aperture and permeability | *Andreani et al.* [2008] |
| Mudstone, Krechba Field, In Salah, Algeria | Flow-through experiments (permeameter) | Quartz, detrital mica, detrital clay (likely Fe-rich 7 Å clay and illite-smectite) with minor feldspar and oxide phases | Dissolution of the minerals chlorite and siderite | Increasing pore throat radii, porosity increased from 7 to 10%, and increasing permeability by approximately a factor of 8 | *Armitage et al.* [2013] |

changes in mechanical properties, but the mechanical parameters measured for this type of test are not directly suitable as input to mechanical models.

### 8.3.2. $CO_2$-Smectite Interactions and Clay Swelling

Smectite is a group of minerals consisting of an octahedral sheet sandwiched between two tetrahedral sheets and found to varying degree in mudstones and shales. In the interlayers between the sandwiches, surfaces are negative, and positively charged ions (cations) are therefore attracted. In the presence of water, these cations tend to hydrate and increase in volume, and this leads to an expansion of the whole smectite structure. The swelling/shrinking property of smectites is commonly seen in soils. When a clay-rich soil dries out, it shrinks and cracks into polygonal patterns, whereas the soil expands and the cracks close when water is added. Similar fracturing may potentially happen at the base of a seal if dry or near-dry $CO_2$ is allowed to interact with the shale/mudstone and dry out the smectites [*De Jong et al*., 2014; *Busch et al*., 2016]. This will depend on the water content of the $CO_2$, but the exact shrinking/swelling property is complex and is not a linear function of water content. Although still debated, *Loring et al*. [2014] showed that the sorbed water content of Na-montmorillonite increases nearly linear with water content in the $CO_2$, whereas the smectite swells in a stepwise manner with three distinct plateau $d_{001}$ (d-spacing perpendicular to the sheets) values. The reverse reactions were not attempted so any hysteresis effects are not known. The stepwise swelling is also known from traditional experiments using air moisture content and is referred to as crystalline swelling, where there are a number of discrete stable values of layer spacing [e.g., *Morodome and Kawamura*, 2009]. Also, $CO_2$ itself contributes to the volume increases of smectites. $CO_2$ will be incorporated into the layered structure of smectites in the same interlayers as the cations (a process referred to as intercalation), and the structure will swell [*Fripiat et al*., 1974; *Michels et al*., 2015]. The size of the interlaminar ions provides restrictions on the degree of $CO_2$ inclusion, and only the smectites saturated with the larger monovalent cations (including K- and Na-smectites) will allow complete or nearly complete $CO_2$ inclusion [*Fripiat et al*., 1974]. Clay swelling as a self-limiting process within a caprock in a $CO_2$ system is not well understood, although some attempts have been made following the $CO_2$ sorption in clays discussed by *Busch et al*. [2008]. Clay swelling experiments [*Giesting et al*., 2012; *Schaef et al*., 2012; *De Jong et al*., 2014] show that $scCO_2$ has the potential for mechanical swelling of smectite as function of the clays initial hydration stage. For smectite-rich caprocks, swelling may influence fracture closure and healing [*Bastiaens et al*., 2007; *Zhang*, 2011], whereas the effect of swelling stress induced by $CO_2$ sorption is less well understood [*Busch et al*., 2016].

### 8.3.3. Carbonate-Cemented Fractures

Both carbonate- and gypsum-cemented veins related to paleo-leakage and active $CO_2$ leakage are observed in the Green River area, Utah [*Dockrill and Shipton*, 2010; *Kampman et al*., 2012]. Calcite precipitates rapidly from solutions supersaturated with $CaCO_3$ (if not inhibited by, e.g., Mg) and responds rapidly to changing thermodynamic conditions. Brines in the Green River area are found to be Mg rich, which might explain the formation of aragonite over calcite [*Kampman et al*., 2012]. Calcite is getting more stable as temperature increases, and a heating of a saturated aqueous solution will therefore lead to precipitation; however, for the aragonite veins in Green River, precipitation is found to take place due to outgassing of the local system [*Kampman et al*., 2012]. The calcite solubility is also a function of $CO_2$ pressure, and more calcite can be dissolved at higher $CO_2$ pressures, whereas the source for calcium in the system can be local from, for example, feldspar dissolving from rock matrix or transported into the system by the fluid. Carbonate veins can also be present in clay-rich caprocks, like the Kimmeridge shale [*Gutierrez et al*., 2000]. These veins may provide pathways for $CO_2$ within the caprock if not fully sealed or if reactivated. If water-saturated $CO_2$ (or a $CO_2$-charged solution with high $CO_2$ partial pressure) is migrating into calcite-filled fractures, reopened by an overpressure, the existing calcite will to some extent dissolve and lead to permeability increase. However, because of the fast kinetics, solutions are soon saturated with calcite at higher aqueous $Ca^{2+}$, and the dissolution will cease.

Experimental work focusing on carbonate cement in fractures is mainly concerned with the dissolution of calcite and addressing the alteration in flow properties due to $CO_2$-saturated fluids in typical caprock materials [*Andreani et al*., 2008; *Ellis et al*., 2011; *Ellis et al*., 2013]. Based on experimental results, it is observed that the effects of calcite dissolution, increasing porosity, and changes in transport properties are complex. The alteration experiments on fractured claystone by *Andreani et al*. [2008] show dissolution of quartz and calcite increasing the fracture porosity, whereas the permeability remains unchanged. This lack of effect on permeability is attributed to remaining clay framework and limited net effects on the fracture aperture. Cyclic $CO_2$-brine and $CO_2$-gas flow on the same material showed an increase in aperture explained by clay particle decohesion, and clay particles are wrenched from the fracture surface [*Andreani et al*., 2008].

### 8.3.4. Dry $CO_2$: Fracture-Brine Interactions

Dry $CO_2$ has the potential to dry out fracture walls, and if the fracture water is brine, salt may precipitate. The risk of dry $CO_2$ in contact with the caprock is debated and not considered likely.

To what extent such dry-outs may occur in the caprock depends on the initial water content of the $CO_2$ and the volume of $CO_2$ that migrates through the fracture. The degree of dry-out also depends on the possibility of water to be supplied from the shale/mudstone matrix. Whether total dry-out or not may occur, salt may form rapidly as soon as the saturation limit of the water with respect to halite (NaCl) is reached. This has been shown numerically for the near-well area in the reservoir [*Miri et al*., 2015] and also suggested from injectivity losses in $CO_2$ injection operations at Snøhvit [*Grude et al*., 2014] and Ketzin [*Baumann et al*., 2014]. Salt formation in fractured systems has been less studied. *Miri et al*. [2015] studied the process of salt precipitation at the pore scale by performing experiments in a microchip as shown close up in Figure 8.6. The microchip can be considered a dual-porosity medium, where the simulated fracture serves as a region dried by $CO_2$ and the connected porous medium reflects the water-saturated matrix. Salt growth was initiated at the interface, but directed into the $CO_2$-rich phase. Rapid nucleation leads to the formation of massive porous aggregates of micrometer-sized crystals. This growth then proceeded to fill the entire fracture width, and fracture flow was significantly reduced. In the case of complete clogging, the dry-out may provide a strong negative feedback to the flow, hindering the likelihood of $CO_2$ leakage. The experiments were, however, performed in a microfluidic system representing a fractured permeable sand rather than shale/mudstone, and similar experiments must also be done on a tight rock before any conclusions can be made.

### 8.3.5. Shear Fractures and Frictional Properties

Effects of $CO_2$ alteration on material properties like cohesion and friction of faults and fractures should be evaluated for longtime storage. Data from laboratory tests and field observations show that friction coefficients generally vary between 0.6 and 0.85 [*Byerlee*, 1978; *Morrow et al*., 1992], although values as low as 0.2 have also been reported for clay material in the literature. Natural faults and shear fractures often contain gouge, so the friction is strongly dependent on the mineral composition of the gouge [*Moore and Lockner*, 1995; *Tembe et al*., 2010; *Samuelson and Spiers*, 2012] and decreases with increasing the bulk clay content. The type of fluid in the sliding surface will also influence friction, with water-wet surfaces decreasing the friction coefficient. Influence of $scCO_2$- and $CO_2$-saturated brine on frictional properties and slip velocities of fault gauges has been investigated experimentally. Rate and state frictional experiments were performed for clastic caprock material dominated by illite, quartz, and quartz-rich reservoir material [*Samuelson and Spiers*, 2012], showing that $scCO_2$ had no clear influence on frictional strength of dry or brine-saturated gouges. For a full overview of $CO_2$-related work on fault stability and reactivation, see *Rohmer et al*. [2016] and discussions therein.

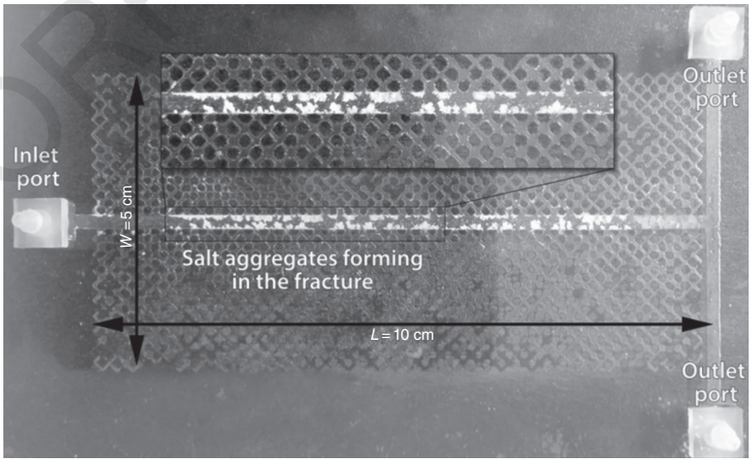


**Figure 8.6** Pore-scale visualization of salt precipitation in the preferential pathway (fracture) of the heterogeneous microchip. After *Miri et al*. [2015]. A thick film of brine remains after $CO_2$ invasion at 5 s after injection. After 50 min, this film evaporates and the drying front shapes a meniscus at the interface between matrix and fracture. After 75 min, aggregation growth starts and occupies the fractures. AQ3

## 8.4. EXAMPLES FROM SEALING UNITS IN THE NORTH SEA

In the North Sea, the Sleipner $CO_2$ injection project has successfully injected more than 16 Mt. $CO_2$ since it was started in 1996 [*Furre et al*., 2017]. At Sleipner, $CO_2$ is injected into the Utsira sand, and the regional extensive Pliocene to Pleistocene Nordland Shale is the caprock. The Utsira sand has been considered to have sufficient capacity to store $CO_2$ emissions from large part of the European industry (150 Gt/year) for several decades [*Ramírez et al*., 2011]. Recent Norwegian feasibility studies have identified storage potential in the Sognefjord Formation, east of the Troll gas field in the North Sea. The primary seal for this unit is the Upper Jurassic Draupne Formation. In the following, the Nordland Shale and Draupne Formation will be discussed in more detail.

### 8.4.1. Nordland Shale

The Nordland Shale is only weakly consolidated because of the shallow burial (maximum ~800–1000 m) and consists mainly of clay and silt with some minor sands and with weak bedding [*Gregersen and Johannessen*, 2001; *Pillitteri et al*., 2003]. The seal has been divided into three units: the lower seal draping the Utsira sand, the middle-down-lapping seal, and finally the upper seal with a truncated lower boundary [*Gregersen and Johannessen*, 2001]. *Bøe* and *Zweigel* [2001] estimated the pore throat radius and found that a $CO_2$ column of more than 800 m is required for capillary failure, and no free-phase $CO_2$ transport is therefore expected into the lower intact seal. A similar result was found by *Harrington et al*. [2009], concluding that only pressure-induced flow pathways (i.e., fractures) are relevant for seal breach because of the high gas breakthrough pressures for the intact caprock. However, the observed transport of $CO_2$ through thin intra-reservoir mudstone layers [*Zweigel et al*., 2004] has raised discussions about the transport of $CO_2$ through the shale barriers. Diffusive transport through the seal will be slow, and significant amounts of plagioclase and chlorite in the caprock [*Bøe and Zweigel*, 2001] may react and have potential to bind $CO_2$ [*Pham et al*., 2011; *Hellevang and Aagaard*, 2013], further slowing down diffusive transport of $CO_2$ through the seal.

The present-day $CO_2$ injection at Sleipner generates an overpressure that is <0.1 MPa [*Chadwick et al*., 2012], making reservoir and seal pressurization a low risk. In addition, triaxial tests suggest that the lower seal is elastic-perfectly plastic, with Young's moduli measured to 0.19–0.29 GPa and Poisson's ratio of 0.18–0.25 [*Pillitteri et al*., 2003], indicating that fracturing is unlikely. The vertical effective stress was found to be significantly larger than the horizontal, and it was also found that the vertical effective stress was larger than explained by the present-day overburden. This suggests over-consolidation of the sediments related to the Quaternary ice sheet loading in the North Sea. Capillary flow simulations including a fractured shale barrier were presented to replicate the monitored plume development [*Cavanagh and Haszeldine*, 2014], suggesting fracturing that predates the $CO_2$ injection explained as transient pore pressure hydro-fracturing during the deglaciation. Current plume monitoring program identifies a total of 9 $CO_2$ horizons separated by thin shale layers, typically 1–1.5 m thick, and one thicker layer of ca 6 m was identified [*Furre et al*., 2017]. The data from Sleipner $CO_2$ project have been used for a wide variety of flow simulations [e.g., *Cavanagh*, 2013]. Geological assumptions about the nature and number of feeder channels for $CO_2$ from the injection point and up to the top layer where $CO_2$ accumulates are highly uncertain for current simulations [*Furre et al*., 2017] and represent a key challenge for the future.

### 8.4.2. Draupne Formation

The Upper Jurassic Draupne Formation forms a several hundred meter thick source rock, but also a good seal for deeper reservoirs. Equivalent Upper Jurassic formation is the Kimmeridge Clay Formation, but also Spekk, Mandal, and Tau formations are approximate equates [*Faleide et al*., 2015]. Recently, 9 m of well-preserved core material from the Draupne Formation within the Ling Depression was made available for $CO_2$-related research on seal integrity in the North Sea. The low permeability and high $CO_2$ capillary breakthrough pressure suggest this to be an excellent caprock [*Skurtveit et al*., 2012; *Skurtveit et al*., 2015]. Mineralogy of intact shale shows a bulk composition of quartz, microcline, and clay, with the clay phase dominated by kaolinite and smectite and total organic carbon around 7–8%. Along a natural shear fracture observed in the upper section of the core, increased calcite, pyrite, and siderite content is found compared to the intact shale mineralogy. Main uncertainty for the sealing capacity evaluation of this formation is related to the observed natural shear fracture, where the capillary entry pressure could be lower and the permeability could be higher than for the intact material. There are no indications that the observed shear fractures are common for the Draupne Formation, nor that they are continuous throughout the thickness of the seal; however, the samples provide excellent core material for further investigation of natural shear fractures in clay-rich seal. Potential reactions for $CO_2$ percolation into fractured Draupne Formation include calcite dissolution [e.g., *Alemu et al*., 2011] that might alter the porosity

[*Andreani et al*., 2008], whereas mobilization of less soluble particles or swelling of smectite may result in clogging and sealing of the fracture as demonstrated experimentally by *Bastiaens et al*. [2007] and *Ellis et al*. [2013].

## 8.5. CONCLUDING REMARKS AND FUTURE DIRECTIONS

Dedicated research on $CO_2$ storage and related fluid-rock interaction processes has provided insight and new data on transport and reactions to be expected for both reservoirs and sealing units. This review, focusing on flow and alteration processes in clay-rich seals (Fig. 8.1), showed that the most likely transport of $CO_2$ into clay-rich seal is by diffusion and only the lower 1–10 m of a typical clay seal will be affected. Flow of $CO_2$ into the seal is only likely if the seal is damaged due to preexisting fractures or faults within the seal. However, the long-term effects of alteration are an essential part of a storage system, and fluid-rock interaction processes may be important for leakage mitigation and as remediation strategies [*Kim and Santamarina*, 2013; *Tongwa et al*., 2013; *Druhan et al*., 2014; *Vialle et al*., 2016].

Reaction experiments and kinetic modeling show reactivity between $CO_2$-saturated fluids (acidic) and clay-rich caprock material, involving kaolinite precipitation and chlorite-to-ankerite transformation. However, for dominating clay-rich caprock minerals like quartz, illite, and smectite, the reactivity due to drop in pH is low. Carbonate-rich shale is found to be more reactive than clay-rich shale; however, reactions may also be buffered depending on the fluid composition and water-rock ratio. For the experiments and models available, only minor porosity changes are observed, and implications for flow and $CO_2$ transport are uncertain due to limited data available, slow reaction rates, and low flow rates in clay-rich seals. Important alteration processes applicable for clay-rich caprocks include the swelling and shrinking property of smectites due to $CO_2$ sorption, where limited data are available. Clay swelling due to $CO_2$ raises an interesting discussion about the possibilities for self-limiting processes in clay-rich seal; however, a better understanding of the difference in amount of swelling between $CO_2$ and water and possible interaction effects is needed to fully understand the implications for $CO_2$ transport. Special cases of $CO_2$ transport in fractured caprock discussed in this paper include carbonate-cemented fractures, the possibility for salt precipitation resulting from entering of dry $CO_2$, and $CO_2$ effects on frictional properties of clay-rich gauge. The main finding is that there is very little work dedicated to effects of $CO_2$ in fractured clay-rich seals. It can be argued that damaged seals with extensive fracturing and faulting should be avoided; however, in order to perform proper risk evaluation of clay-rich caprocks, the process involved needs to be understood and discussed.

This review identifies several challenges related to the dynamic interaction and coupling of processes and research approaches. The available experimental data are difficult to upscale and extrapolate both in time and space. The time frame during laboratory experiments is different from reservoir conditions, and pressure and temperature conditions are adjusted to speed up the reactions. Alteration experiments might have unrealistic supply of reactive fluids, and the heterogeneities of a system might not be captured in a single experiment. Some important research gaps and processes that require a better understanding in order to secure the long-term safety of $CO_2$ sequestration are suggested for further investigation:

- Extrapolation between laboratory experiments and field observations to verify the rates and complexity used for kinetic modeling of reaction potential within sealing units and to document the net effect of alteration on transport properties
- More experimental data on clay-rich caprocks and models specifically addressing effect of clay swelling and dissolution of organic matter in a brine-$CO_2$ system
- Fracture transmissibility and the hydromechanical-chemical coupling of single fractures and fracture network for two-phase flow involving $CO_2$
- Long-term effects of $CO_2$ on frictional stability of clay-rich gauge and their mechanical and transport properties

## ACKNOWLEDGMENTS

This work has been funded by Research Council of Norway (RCN) under the $CO_2$ seal bypass project (grant no. 244049) and by the FME SUCCESS Centre (grant 193825/S60). FME SUCCESS is a consortium with partners from industry and science, hosted by Christian Michelsen Research AS. The work by Elin Skurtveit is also supported by NGI internal funding. Bahman Bohloli is thanked for helpful comments on an early version of the manuscript. Two anonymous reviewers and editor, Stèphanie Vialle, are thanked for their detailed input significantly improving the manuscript.

## REFERENCES

Alemu, B. L., P. Aagaard, I. A. Munz, and E. Skurtveit (2011), Caprock interaction with $CO_2$: A laboratory study of reactivity of shale with supercritical $CO_2$ and brine, *Applied Geochemistry*, *26*(12), 1975–1989, doi:10.1016/j.apgeochem.2011.06.028.

Andreani, M., P. Gouze, L. Luquot, and P. Jouanna (2008), Changes in seal capacity of fractured claystone caprocks induced by dissolved and gaseous $CO_2$ seepage, *Geophysical Research Letters*, *35*(14), L14404.

Angeli, M., M. Soldal, E. Skurtveit, and E. Aker (2009), Experimental percolation of supercritical $CO_2$ through a caprock, *Energy Procedia*, *1*(1), 3351–3358.

Armitage, P., D. Faulkner, R. Worden, A. Aplin, A. Butcher, and J. Iliffe (2011), Experimental measurement of, and controls on, permeability and permeability anisotropy of caprocks from the $CO_2$ storage project at the Krechba field, Algeria, *Journal of Geophysical Research - Solid Earth*, *116*(B12), B12208.

Armitage, P., D. Faulkner, and R. Worden (2013), Caprock corrosion, *Nature Geoscience*, *6*(2), 79–80.

Balashov, V. N., G. D. Guthrie, C. L. Lopano, J. A. Hakala, and S. L. Brantley (2015), Reaction and diffusion at the reservoir/shale interface during $CO_2$ storage: Impact of geochemical kinetics, *Applied Geochemistry*, *61*, 119–131.

Bandis, S., A. Lumsden, and N. Barton (1983), Fundamentals of rock joint deformation, paper presented at International Journal of Rock Mechanics and Mining Sciences & Geomechanics Abstracts, Elsevier.

Barenblatt, G., I. P. Zheltov, and I. Kochina (1960), Basic concepts in the theory of seepage of homogeneous liquids in fissured rocks [strata], *Journal of Applied Mathematics and Mechanics*, *24*(5), 1286–1303.

Barton, N., S. Bandis, and K. Bakhtar (1985), Strength, deformation and conductivity coupling of rock joints, paper presented at International Journal of Rock Mechanics and Mining Sciences & Geomechanics Abstracts, Elsevier.

Bastiaens, W., F. Bernier, and X. L. Li (2007), SELFRAC: Experiments and conclusions on fracturing, self-healing and self-sealing processes in clays, *Physics and Chemistry of the Earth, Parts A/B/C*, *32*(8), 600–615.

Baumann, G., J. Henninges, and M. De Lucia (2014), Monitoring of saturation changes and salt precipitation during $CO_2$ injection using pulsed neutron-gamma logging at the Ketzin pilot site, *International Journal of Greenhouse Gas Control*, *28*, 134–146.

Berre, T. (2011), Triaxial testing of soft rocks, *Geotechnical Testing Journal*, *34*(1), 61–75.

Bird, R. B. (2002), Transport phenomena, *Applied Mechanics Reviews*, *55*(1), R1–R4.

Bøe, R., and P. Zweigel (2001), Characterisation of the Nordland Shale in the Sleipner area by XRD analysis – a contribution to the Saline Aquifer $CO_2$ Storage (SACS) project. Confidential SINTEF Report 33.0764.00/01/01.

Boulin, P., P. Bretonnier, V. Vassil, A. Samouillet, M. Fleury, and J. Lombard (2013), Sealing efficiency of caprocks: Experimental investigation of entry pressure measurement methods, *Marine and Petroleum Geology*, *48*, 20–30.

Brush, D. J., and N. R. Thomson (2003), Fluid flow in synthetic rough-walled fractures: Navier-Stokes, stokes, and local cubic law simulations, *Water Resources Research*, *39*(4), 1085.

Busch, A., S. Alles, Y. Gensterblum, D. Prinz, D. N. Dewhurst, M. D. Raven, H. Stanjek, and B. M. Krooss (2008), Carbon dioxide storage potential of shales, *International Journal of Greenhouse Gas Control*, *2*(3), 297–308.

Busch, A., A. Amann-Hildenbrand, P. Bertier, M. Waschbuesch, and B. M. Krooss (2010), The significance of caprock sealing integrity for $CO_2$ storage, paper presented at SPE International Conference on $CO_2$ Capture, Storage, and Utilization, Society of Petroleum Engineers.

Busch, A., N. Kampman, S. Hangx, J. Snippe, M. Bickle, P. Bertier, H. Chapman, C. Spiers, R. Pijnenburg, and J. Samuelson (2014), The Green River natural analogue as a field laboratory to study the long-term fate of $CO_2$ in the subsurface, *Energy Procedia*, *63*, 2821–2830.

Busch, A., P. Bertier, Y. Gensterblum, G. Rother, C. Spiers, M. Zhang, and H. Wentinck (2016), On sorption and swelling of $CO_2$ in clays, *Geomechanics and Geophysics for Geo-Energy and Geo-Resources*, *2*(2), 111–130.

Byerlee, J. (1978), Friction of rocks, *Pure and Applied Geophysics*, *116*(4–5), 615–626.

Carey, J. W., Z. Lei, E. Rougier, H. Mori, and H. Viswanathan (2015), Fracture-permeability behavior of shale, *Journal of Unconventional Oil and Gas Resources*, *11*, 27–43.

Carroll, S. A., W. W. McNab, and S. C. Torres (2011), Experimental study of cement-sandstone/shale-brine-$CO_2$ interactions, *Geochemical Transactions*, *12*(1), 9.

Cavanagh, A. (2013), Benchmark calibration and prediction of the Sleipner $CO_2$ plume from 2006 to 2012, *Energy Procedia*, *37*, 3529–3545.

Cavanagh, A., and R. S. Haszeldine (2014), The Sleipner storage site: Capillary flow modeling of a layered $CO_2$ plume requires fractured shale barriers within the Utsira formation, *International Journal of Greenhouse Gas Control*, *21*, 101–112.

Chadwick, R., G. Williams, J. Williams, and D. Noy (2012), Measuring pressure performance of a large saline aquifer during industrial-scale $CO_2$ injection: The Utsira Sand, Norwegian North Sea, *International Journal of Greenhouse Gas Control*, *10*, 374–388.

Chareonsuppanimit, P., S. A. Mohammad, R. L. Robinson, and K. A. Gasem (2012), High-pressure adsorption of gases on shales: Measurements and modeling, *International Journal of Coal Geology*, *95*, 34–46.

Chiaramonte, L., J. A. White, and W. Trainor-Guitton (2015), Probabilistic geomechanical analysis of compartmentalization at the Snøhvit $CO_2$ sequestration project, *Journal of Geophysical Research - Solid Earth*, *120*(2), 1195–1209.

Chiquet, P., D. Broseta, and S. Thibeau (2007), Wettability alteration of caprock minerals by carbon dioxide, *Geofluids*, *7*(2), 112–122.

Cho, Y., E. Ozkan, and O. G. Apaydin (2013), Pressure-dependent natural-fracture permeability in shale and its effect on shale-gas well production, *SPE Reservoir Evaluation & Engineering*, *16*(2), 216–228.

De Jong, S., C. Spiers, and A. Busch (2014), Development of swelling strain in smectite clays through exposure to carbon dioxide, *International Journal of Greenhouse Gas Control*, *24*, 149–161.

Dockrill, B., and Z. K. Shipton (2010), Structural controls on leakage from a natural $CO_2$ geologic storage site: Central Utah, USA, *Journal of Structural Geology*, *32*(11), 1768–1782.

Druhan, J. L., S. Vialle, K. Maher, and S. Benson (2014), A reactive transport model for geochemical mitigation of $CO_2$ leaking into a confined aquifer, *Energy Procedia*, *63*, 4620–4629.

Edlmann, K., S. Haszeldine, and C. McDermott (2013), Experimental investigation into the sealing capability of naturally fractured shale caprocks to supercritical carbon dioxide flow, *Environment and Earth Science*, *70*(7), 3393–3409.

Ellis, B. R., G. S. Bromhal, D. L. McIntyre, and C. A. Peters (2011), Changes in caprock integrity due to vertical migration of $CO_2$-enriched brine, *Energy Procedia*, *4*, 5327–5334.

Ellis, B. R., J. P. Fitts, G. S. Bromhal, D. L. McIntyre, R. Tappero, and C. A. Peters (2013), Dissolution-driven permeability reduction of a fractured carbonate caprock, *Environmental Engineering Science*, *30*(4), 187–193.

Espinoza, D. N., and J. C. Santamarina (2012), Clay interaction with liquid and supercritical $CO_2$: The relevance of electrical and capillary forces, *International Journal of Greenhouse Gas Control*, *10*, 351–362.

Faleide, J. I., K. Bjørlykke, and R. H. Gabrielsen (2015), Geology of the Norwegian continental shelf, in K. Bjørlykke (ed.), *Petroleum Geoscience: From Sedimentary Environments to Rock Physics*, pp. 603–637, Springer Verlag, Berlin Heidelberg.

Faulkner, D., C. Jackson, R. Lunn, R. Schlische, Z. K. Shipton, C. Wibberley, and M. Withjack (2010), A review of recent developments concerning the structure, mechanics and fluid flow properties of fault zones, *Journal of Structural Geology*, *32*(11), 1557–1575.

Festoy, S., and V. Golf-Racht (1989), Gas gravity drainage in fractured reservoirs through new dual-continuum approach (includes associated papers 20296 and 20390), *SPE Reservoir Engineering*, *4*(3), 271–278.

Fripiat, J., M. Cruz, B. Bohor, and J. Thomas Jr (1974), Interlamellar adsorption of carbon dioxide by smectites, *Clays and Clay Minerals*, *22*(1), 23–30.

Furre, A.-K., O. Eiken, H. Alnes, J. N. Vevatne, and A. F. Kiær (2017), 20 Years of monitoring $CO_2$-injection at Sleipner, *Energy Procedia*, *114*, 3916–3926, doi:10.1016/j.egypro.2017.03.1523.

Gaus, I., M. Azaroual, and I. Czernichowski-Lauriol (2005), Reactive transport modelling of the impact of $CO_2$ injection on the clayey cap rock at Sleipner (North Sea), *Chemical Geology*, *217*(3), 319–337.

Gherardi, F., T. Xu, and K. Pruess (2007), Numerical modeling of self-limiting and self-enhancing caprock alteration induced by $CO_2$ storage in a depleted gas reservoir, *Chemical Geology*, *244*(1), 103–129.

Giesting, P., S. Guggenheim, A. F. K. van Groos, and A. Busch (2012), Interaction of carbon dioxide with Na-exchanged montmorillonite at pressures to 640bars: Implications for $CO_2$ sequestration, *International Journal of Greenhouse Gas Control*, *8*, 73–81.

Gregersen, U., and P. Johannessen (2001), The Neogene Utsira sand and its seal in the Viking Graben area, North Sea saline aquifer $CO_2$ storage (SACS) project, phase 2 task 1.7 geology, *Geological Survey of Denmark and Greenland Report*, *100*(2001), 1–2.

Grude, S., M. Landrø, and J. Dvorkin (2014), Pressure effects caused by $CO_2$ injection in the Tubåen Fm., the Snøhvit field, *International Journal of Greenhouse Gas Control*, *27*, 178–187.

Gutierrez, M., L. Øino, and R. Nygård (2000), Stress-dependent permeability of a de-mineralised fracture in shale, *Marine and Petroleum Geology*, *17*(8), 895–907.

Hangx, S., A. van der Linden, F. Marcelis, and A. Bauer (2013), The effect of $CO_2$ on the mechanical properties of the captain sandstone: Geological storage of $CO_2$ at the Goldeneye field (UK), *International Journal of Greenhouse Gas Control*, *19*, 609–619.

Harrington, J., and S. Horseman (1999), Gas transport properties of clays and mudrocks, *Geological Society, London, Special Publications*, *158*(1), 107–124.

Harrington, J. F., D. J. Noy, S. T. Horseman, D. J. Birchall, and R. A. Chadwick (2009), Laboratory study of gas and water flow in the Nordland Shale, Sleipner, North Sea, in M. Grobe, J. C. Pashin, and R. L. Dodge (eds.), *Carbon Dioxide Sequestration in Geological Media – State of the Science*, AAPG Studies in Geology 59, p. 521–543.

Hellevang, H. (2006), Interactions between $CO_2$, saline water and minerals during geological storage of $CO_2$, PhD thesis, The University of Bergen.

Hellevang, H., and P. Aagaard (2013), Can the long-term potential for carbonatization and safe long-term $CO_2$ storage in sedimentary formations be predicted?, *Applied Geochemistry*, *39*, 108–118.

Hellevang, H., V. T. Pham, and P. Aagaard (2013), Kinetic modelling of $CO_2$–water–rock interactions, *International Journal of Greenhouse Gas Control*, *15*, 3–15.

Hildenbrand, A., S. Schlömer, B. Krooss, and R. Littke (2004), Gas breakthrough experiments on pelitic rocks: Comparative study with $N_2$, $CO_2$ and $CH_4$, *Geofluids*, *4*(1), 61–80.

Ishii, E. (2015), Predictions of the highest potential transmissivity of fractures in fault zones from rock rheology: Preliminary results, *Journal of Geophysical Research - Solid Earth*, *120*(4), 2220–2241.

Jaeger, J. C., N. G. Cook, and R. Zimmerman (2009), *Fundamentals of Rock Mechanics*, Hoboken, NJ, John Wiley & Sons.

Kampman, N., N. M. Burnside, Z. K. Shipton, H. J. Chapman, J. A. Nicholl, R. M. Ellam, and M. J. Bickle (2012), Pulses of carbon dioxide emissions from intracrustal faults following climatic warming, *Nature Geoscience*, *5*(5), 352–358.

Kampman, N., A. Maskell, M. Bickle, J. Evans, M. Schaller, G. Purser, Z. Zhou, J. Gattacceca, E. Peitre, and C. Rochelle (2013), Scientific drilling and downhole fluid sampling of a natural $CO_2$ reservoir, Green River, Utah, *Scientific Drilling*, *16*, 33–43.

Kampman, N., M. Bickle, A. Maskell, H. Chapman, J. Evans, G. Purser, Z. Zhou, M. Schaller, J. C. Gattacceca, and P. Bertier (2014a), Drilling and sampling a natural $CO_2$ reservoir: Implications for fluid flow and $CO_2$-fluid–rock reactions during $CO_2$ migration through the overburden, *Chemical Geology*, *369*, 51–82.

Kampman, N., M. Bickle, M. Wigley, and B. Dubacq (2014b), Fluid flow and $CO_2$–fluid–mineral interactions during $CO_2$-storage in sedimentary basins, *Chemical Geology*, *369*, 22–50.

Kaszuba, J. P., D. R. Janecky, and M. G. Snow (2005), Experimental evaluation of mixed fluid reactions between supercritical carbon dioxide and NaCl brine: Relevance to the integrity of a geologic carbon repository, *Chemical Geology*, *217*(3), 277–293.

Kim, S., and J. C. Santamarina (2013), $CO_2$ breakthrough and leak-sealing – experiments on shale and cement, *International Journal of Greenhouse Gas Control*, *19*, 471–477.

Le Guen, Y., F. Renard, R. Hellmann, E. Brosse, M. Collombet, D. Tisserand, and J. P. Gratier (2007), Enhanced deformation

of limestone and sandstone in the presence of high fluids, *Journal of Geophysical Research - Solid Earth*, *112*(B5), B05421.

Lim, K., and K. Aziz (1995), Matrix-fracture transfer shape factors for dual-porosity simulators, *Journal of Petroleum Science and Engineering*, *13*(3), 169–178.

de Lima, V., S. Einloft, J. M. Ketzer, M. Jullien, O. Bildstein, and J.-C. Petronin (2011), $CO_2$ geological storage in saline aquifers: Paraná Basin caprock and reservoir chemical reactivity, *Energy Procedia*, *4*, 5377–5384.

Liu, F., P. Lu, C. Griffith, S. W. Hedges, Y. Soong, H. Hellevang, and C. Zhu (2012), $CO_2$–brine–caprock interaction: Reactivity experiments on Eau Claire shale and a review of relevant literature, *International Journal of Greenhouse Gas Control*, *7*, 153–167.

Loring, J. S., E. S. Ilton, J. Chen, C. J. Thompson, P. F. Martin, P. Bénézeth, K. M. Rosso, A. R. Felmy, and H. T. Schaef (2014), In Situ study of $CO_2$ and $H_2O$ partitioning between Na–Montmorillonite and variably wet supercritical carbon dioxide, *Langmuir*, *30*(21), 6120–6128.

Lu, J., M. Wilkinson, R. S. Haszeldine, and A. E. Fallick (2009), Long-term performance of a mudrock seal in natural $CO_2$ storage, *Geology*, *37*(1), 35–38.

Mao, Y., M. Zeidouni, and R. Askari (2017), Effect of leakage pathway flow properties on thermal signal associated with the leakage from $CO_2$ storage zone, *Greenhouse Gases: Science and Technology*, *7*(3), 512–529.

McCain, W. D. (1990), *The Properties of Petroleum Fluids*, Tulsa, OK, PennWell Books.

Michels, L., J. O. Fossum, Z. Rozynek, H. Hemmen, K. Rustenberg, P. A. Sobas, G. N. Kalantzopoulos, K. Knudsen, M. Janek, and T. Plivelic (2015), Intercalation and Retention of Carbon Dioxide in a Smectite Clay Promoted by Interlayer Cations. Scientific Reports, 5.

Miri, R., P. Aagaard, and H. Hellevang (2014a), Examination of $CO_2$–$SO_2$ solubility in water by SAFT1. Implications for $CO_2$ transport and storage, *The Journal of Physical Chemistry B*, *118*(34), 10214–10223.

Miri, R., H. Hellevang, A. Braathen, and P. Aagaard (2014b), Phase relations in the Longyearbyen $CO_2$ lab reservoir-forecasts for $CO_2$ injection and migration, *Norwegian Journal of Geology*, *94*(2–3), 217–232.

Miri, R., R. v. Noort, P. Aagaard, and H. Hellevang (2015), New insights on the physics of salt precipitation during injection of $CO_2$ into saline aquifers, *International Journal of Greenhouse Gas Control*, *43*, 10–21.

Moore, D. E., and D. Lockner (1995), The role of microcracking in shear-fracture propagation in granite, *Journal of Structural Geology*, *17*(1), 95–114.

Morodome, S., and K. Kawamura (2009), Swelling behavior of Na-and Ca-montmorillonite up to 150 C by in situ X-ray diffraction experiments, *Clays and Clay Minerals*, *57*(2), 150–160.

Morrow, C., B. Radney, and J. Byerlee (1992), Frictional strength and the effective pressure law of Montmorillonite and illite clays, *International Geophysics*, *51*, 69–88.

Mouzakis, K. M., A. K. Navarre-Sitchler, G. Rother, J. L. Bañuelos, X. Wang, J. P. Kaszuba, J. E. Heath, Q. R. Miller, V. Alvarado, and J. E. McCray (2016), Experimental study of porosity changes in shale caprocks exposed to $CO_2$-saturated brines I: Evolution of mineralogy, pore connectivity, pore size distribution, and surface area, *Environmental Engineering Science*, *33*(10), 725–735.

Myer, L. R. (2000), Fractures as collections of cracks, *International Journal of Rock Mechanics and Mining Sciences*, *37*(1), 231–243.

Nordgård Bolås, H. M., C. Hermanrud, and G. M. Teige (2005), Seal capacity estimation from subsurface pore pressures, *Basin Research*, *17*(4), 583–599.

Ogata, K., K. Senger, A. Braathen, and J. Tveranger (2014), Fracture corridors as seal-bypass systems in siliciclastic reservoir-cap rock successions: Field-based insights from the Jurassic Entrada Formation (SE Utah, USA), *Journal of Structural Geology*, *66*, 162–187, doi:10.1016/j.jsg.2014.05.005.

Olivella, S., and E. E. Alonso (2008), Gas flow through clay barriers. *Géotechnique 58*(3), 157–176.

Oron, A. P., and B. Berkowitz (1998), Flow in rock fractures: The local cubic law assumption reexamined, *Water Resources Research*, *34*(11), 2811–2825.

Ougier-Simonin, A., F. Renard, C. Boehm, and S. Vidal-Gilbert (2016), Microfracturing and microporosity in shales, *Earth-Science Reviews*, *162*, 198–226.

Pham, V., P. Lu, P. Aagaard, C. Zhu, and H. Hellevang (2011), On the potential of $CO_2$–water–rock interactions for $CO_2$ storage using a modified kinetic model, *International Journal of Greenhouse Gas Control*, *5*(4), 1002–1015.

Pillitteri, A., P. Cerasi, J. Stavrum, P. Zweigel, and R. Bøe (2003), Rock mechanical tests of shale samples from the cap rock of the Utsira Sand in well 15/9-A11, A contribution to the saline aquifer $CO_2$ Storage (SACS) project, *Rep. 33.5324.00/06/03*, SINTEF Petroleum Research.

Pyrak-Nolte, L., and J. Morris (2000), Single fractures under normal stress: The relation between fracture specific stiffness and fluid flow, *International Journal of Rock Mechanics and Mining Sciences*, *37*(1), 245–262.

Ramírez, A., R. Hoefnagels, M. van den Broek, N. Strachan, A. Fidje, K. Espegren, P. Seljom, M. Blesl, T. Kober, and P. E. Grohnheit (2011), A Comparison of national CCS strategies for Northwest Europe, with a focus on the potential of common $CO_2$ storage at the Utsira formation, *Energy Procedia*, *4*, 2401–2408.

Rathnaweera, T., P. Ranjith, M. Perera, and A. Haque (2016), Influence of $CO_2$–brine Co-injection on $CO_2$ storage capacity enhancement in deep saline aquifers: An experimental study on Hawkesbury sandstone formation, *Energy & Fuels*, *30*(5), 4229–4243.

Renshaw, C. E. (1995), On the relationship between mechanical and hydraulic apertures in rough-walled fractures, *Journal of Geophysical Research - Solid Earth*, *100*(B12), 24629–24636.

Rohmer, J., A. Pluymakers, and F. Renard (2016), Mechano-chemical interactions in sedimentary rocks in the context of $CO_2$ storage: Weak acid, weak effects?, *Earth-Science Reviews*, *157*, 86–110.

Rossen, R., and E. Shen (1989), Simulation of gas/oil drainage and water/oil imbibition in naturally fractured reservoirs, *SPE Reservoir Engineering*, *4*(4), 464–470.

Saidi, A. (1983), Simulation of naturally fractured reservoirs, paper presented at SPE Reservoir Simulation Symposium, Society of Petroleum Engineers.

Samuelson, J., and C. J. Spiers (2012), Fault friction and slip stability not affected by $CO_2$ storage: Evidence from short-term laboratory experiments on North Sea reservoir sandstones and caprocks, *International Journal of Greenhouse Gas Control*, *11*, S78–S90.

Schaef, H. T., E. S. Ilton, O. Qafoku, P. F. Martin, A. R. Felmy, and K. M. Rosso (2012), In situ XRD study of Ca 2+ saturated montmorillonite (STX-1) exposed to anhydrous and wet supercritical carbon dioxide, *International Journal of Greenhouse Gas Control*, *6*, 220–229.

Shipton, Z. K., J. P. Evans, D. Kirschner, P. T. Kolesar, A. P. Williams, and J. Heath (2004), Analysis of $CO_2$ leakage through 'low-permeability' faults from natural reservoirs in the Colorado plateau, east-central Utah, *Geological Society, London, Special Publications*, *233*(1), 43–58.

Skurtveit, E., E. Aker, M. Soldal, M. Angeli, and Z. Wang (2012), Experimental investigation of $CO_2$ breakthrough and flow mechanisms in shale, *Petroleum Geoscience*, *18*(1), 3–15, doi:10.1144/1354-079311-016.

Skurtveit, E., L. Grande, O. Y. Ogebule, R. H. Gabrielsen, J. I. Faleide, N. H. Mondol, R. Maurer, and P. Horsrud (2015), Mechanical testing and sealing capacity of the Upper Jurassic Draupne Formation, North Sea, 49th U.S. Rock Mechanics/Geomechanics Symposium, 28 June–1 July 2015, San Francisco, CA.

Song, J., and D. Zhang (2012), Comprehensive review of caprock-sealing mechanisms for geologic carbon sequestration, *Environmental Science & Technology*, *47*(1), 9–22.

Spycher, N., and K. Pruess (2005), $CO_2$-$H_2O$ mixtures in the geological sequestration of $CO_2$. II. Partitioning in chloride brines at 12–100 C and up to 600 bar, *Geochimica et Cosmochimica Acta*, *69*(13), 3309–3320.

Sun, Y., M. Aman, and D. N. Espinoza (2016), Assessment of mechanical rock alteration caused by $CO_2$–water mixtures using indentation and scratch experiments, *International Journal of Greenhouse Gas Control*, *45*, 9–17.

Szabó, Z., H. Hellevang, C. Király, E. Sendula, P. Kónya, G. Falus, S. Török, and C. Szabó (2016), Experimental-modelling geochemical study of potential CCS caprocks in brine and $CO_2$-saturated brine, *International Journal of Greenhouse Gas Control*, *44*, 262–275.

Tambach, T. J., M. Koenen, L. J. Wasch, and F. van Bergen (2015), Geochemical evaluation of $CO_2$ injection and containment in a depleted gas field, *International Journal of Greenhouse Gas Control*, *32*, 61–80.

Tembe, S., D. A. Lockner, and T. F. Wong (2010), Effect of clay content and mineralogy on frictional sliding behavior of simulated gouges: Binary and ternary mixtures of quartz, illite, and montmorillonite, *Journal of Geophysical Research - Solid Earth*, *115*(B3), B08206.

Tongwa, P., R. Nygaard, A. Blue, and B. Bai (2013), Evaluation of potential fracture-sealing materials for remediating $CO_2$ leakage pathways during $CO_2$ sequestration, *International Journal of Greenhouse Gas Control*, *18*, 128–138.

Tribovillard, N.-P., A. Desprairies, E. Lallier-Vergès, P. Bertrand, N. Moureau, A. Ramdani, and L. Ramanampisoa (1994), Geochemical study of organic-matter rich cycles from the Kimmeridge Clay Formation of Yorkshire (UK): Productivity versus anoxia, *Palaeogeography, Palaeoclimatology, Palaeoecology*, *108*(1–2), 165–181.

Van der Meer, B. (2005), Carbon dioxide storage in natural gas reservoir, *Oil & Gas Science and Technology*, *60*(3), 527–536.

Vialle, S., J. L. Druhan, and K. Maher (2016), Multi-phase flow simulation of $CO_2$ leakage through a fractured caprock in response to mitigation strategies, *International Journal of Greenhouse Gas Control*, *44*, 11–25.

Walsh, J. (1981), Effect of pore pressure and confining pressure on fracture permeability, paper presented at International Journal of Rock Mechanics and Mining Sciences & Geomechanics Abstracts, Elsevier.

Wang, J., and Y. Peng (2014), Numerical modeling for the combined effects of two-phase flow, deformation, gas diffusion and $CO_2$ sorption on caprock sealing efficiency, *Journal of Geochemical Exploration*, *144*, 154–167.

Warren, J., and P. J. Root (1963), The behavior of naturally fractured reservoirs, *Society of Petroleum Engineers Journal*, *3*(3), 245–255.

Washburn, E. W. (1921), The dynamics of capillary flow, *Physical Review*, *17*(3), 273.

Weniger, P., W. Kalkreuth, A. Busch, and B. M. Krooss (2010), High-pressure methane and carbon dioxide sorption on coal and shale samples from the Paraná Basin, Brazil, *International Journal of Coal Geology*, *84*(3), 190–205.

Wollenweber, J., S. Alles, A. Busch, B. Krooss, H. Stanjek, and R. Littke (2010), Experimental investigation of the $CO_2$ sealing efficiency of caprocks, *International Journal of Greenhouse Gas Control*, *4*(2), 231–241.

Xu, T., J. A. Apps, and K. Pruess (2003), Reactive geochemical transport simulation to study mineral trapping for $CO_2$ disposal in deep arenaceous formations, *Journal of Geophysical Research - Solid Earth*, *108*(B2), 2071.

Xu, T., J. A. Apps, and K. Pruess (2005), Mineral sequestration of carbon dioxide in a sandstone–shale system, *Chemical Geology*, *217*(3), 295–318.

Zhang, C.-L. (2011), Experimental evidence for self-sealing of fractures in claystone, *Physics and Chemistry of the Earth, Parts A/B/C*, *36*(17), 1972–1980.

Zimmerman, R. W., and G. S. Bodvarsson (1996), Hydraulic conductivity of rock fractures, *Transport in Porous Media*, *23*(1), 1–30.

Zweigel, P., R. Arts, A. E. Lothe, and E. B. Lindeberg (2004), Reservoir geology of the Utsira Formation at the first industrial-scale underground $CO_2$ storage site (Sleipner area, North Sea), *Geological Society, London, Special Publications*, *233*(1), 165–180.